



ORIGINAL RESEARCH ARTICLE

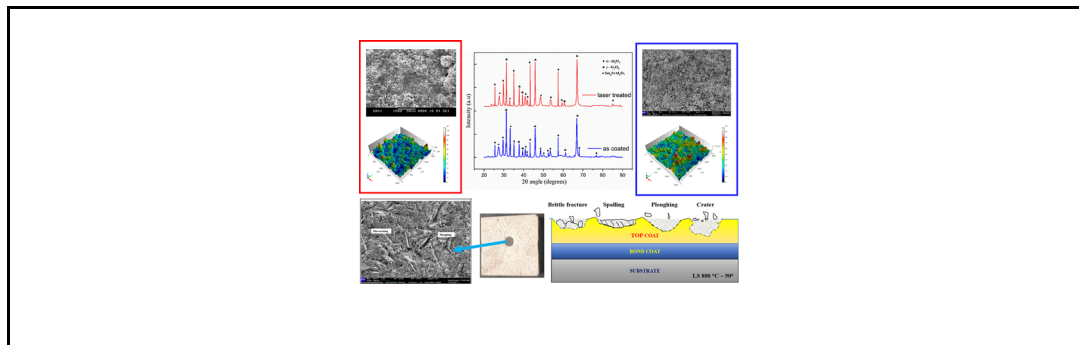
Effect of Surface Modification on Erosion Behavior of Alumina-Samarium Strontium Aluminate Composite Thermal Barrier Coatings

Fredy James J, Shashi Bhushan Arya, S. Yadav, and C.P. Paul

Submitted: 27 March 2023 / Revised: 20 November 2023 / Accepted: 14 December 2023

The mechanical and tribological characteristics of a thermal barrier coating are highly critical in gas turbine applications to resist high-temperature oxidation, corrosion, and solid particle erosion. In the present investigation, a composite coating with alumina and samarium strontium aluminate has been developed through a plasma spraying process. The as-coated composite top coat consisted of three phases α -alumina, γ -alumina, and $\text{Sm}_2\text{SrAl}_2\text{O}_7$. The as-coated surface is re-engineered with an Nd: YAG fiber laser to improve the mechanical and microstructural properties. The laser-treated samples showed a better erosion resistance than the as-coated samples. Despite the surface treatment, both the as-coated and the laser-treated samples showed a higher 'average erosion value' at an impact angle of 90° for the test temperatures of 200 and 800 °C. In addition, the as-coated and the laser-treated samples have a higher erosion rate at 800 than at 200 °C for the selected impact angles, with a mixed mode of material removal presenting both ductile and brittle failure mechanisms.

Graphical Abstract



Keywords composite thermal barrier coatings, erosion mechanism, high-temperature erosion, laser modification, samarium strontium aluminate

1. Introduction

Solid particle erosion is a major failure mechanism of components in thermal power plants, gas turbines, and internal combustion engines, through the presence of particulates of coal, ash, and other harder elements (Ref 1). The erosive impact of

embedded particles in the inlet stream causes thinning of components, changes in blade geometry, and overheating of components in gas turbines (Ref 2). To protect the engine components from erosion and other failure mechanisms such as oxidation and hot corrosion at higher temperatures, thermal barrier coatings (TBCs) are employed. The employed TBC system must be capable of protecting the underlying substrate from the erodent impacts, the resistance being highly dependent on microstructural features, such as open porosities, cracks, and inclusions (Ref 3). Of the various thermal spray techniques, the comparatively simple and cost-effective technique of atmospheric plasma spray (APS) presents a lamellar splat microstructure with unmolten particles, cracks, and porosities, which helps to reduce the thermal conductivity of the coating (Ref 4).

At high temperatures, the most commonly used top coat material yttria-stabilized zirconia (YSZ) undergoes a phase transformation from tetragonal to monoclinic resulting in volume changes, and experience sintering, reducing the strain tolerance and increasing the thermal conductivity (Ref 4, 5) Due to these limitations of conventional YSZ, new coating

J. Fredy James and Shashi Bhushan Arya, Metallurgical and Materials Engineering, National Institute of Technology, Karnataka, Surathkal 575025, India; and S. Yadav and C.P. Paul, Raja Ramanna Centre for Advanced Technology, Indore, Madhya Pradesh 452013, India. Contact e-mail: sbarya@nitk.edu.in.

candidate materials are being studied. The rare earth Lanthanum Zirconate exhibited a better erosion resistance than YSZ coatings, by better hardness (Ref 6). The rare-earth-based RE₂CrTaO₇ ceramic has also been identified as a top coat candidate with higher thermal stability and low thermal conductivity (Ref 7). The single-layer rare earth aluminate Sm₂SrAl₂O₇ has been proven as an alternative to YSZ by its high-temperature stability and corrosion resistance (Ref 8-10).

To date, different multi-layered designs have been studied by various researchers. A single-layered YSZ TBC offered better erosion resistance than a gadolinium zirconate/YSZ double-layered TBC, while a third dense gadolinium zirconate layer showed a better performance than a double-layer design (Ref 11). During operation, these double- and triple-layer coated systems suffer from thermal expansion mismatch and cracking, leading to coating spallation. Rather than double-layer systems, composite coatings may offer better performance at elevated temperatures.

Alumina has been recognized as a coating material with high-temperature stability. Besides pure alumina, fine sapphire powders are used as a coating material because of their chemical inertness and high operating temperatures (Ref 12). Single-layer alumina is reported to have stability issues and spallation at elevated temperatures, while the addition of YSZ has made significant performance improvements. The alumina + YSZ coatings report a higher adhesion strength and better life at a higher alumina content of 65 %, by a dense microstructure and lower porosity level. It also showed a better oxidation resistance with the least thermally grown oxide thickness (Ref 13, 14).

Interestingly, previous works identified that the Al₂O₃ + Sm₂SrAl₂O₇ composite coatings have better hot corrosion resistance in critical aviation conditions, making them a potential candidate for advanced coating systems (Ref 15). The present study investigates the performance of the developed 70 wt.% Al₂O₃-30 wt.% Sm₂SrAl₂O₇ composite TBC against solid particle erosion at temperatures 200 and 800 °C, at impact angles 30° and 90°.

The oxidation, corrosion, and erosion performance of a coating system is highly dependent on the surface characteristics of the coating (Ref 4). Experiments on improving the component performance by sealing the surface porosities through laser treatments have reported advancement in erosion and oxidation resistance, which can be attributed to improved density and reduction in connected cracks and porosities (Ref 3). The laser modification reduces the surface roughness, porosity, and other defects leading to a dense top layer with improved hardness and high-temperature corrosion resistance. Also, a laser-treated YSZ showed a lower spallation tendency at 1100 °C (Ref 16, 17). Depending on the laser parameters employed, fine cracks may be generated in the system without compromising the integrity of the coating, which aids in accommodating the strain leading to better component life (Ref 18). The effect of laser treatment on the high-temperature erosion behavior of the composite coating system is discussed in detail.

2. Experimental Procedure

2.1 Coating Feedstock

The test coupons (20 × 20 × 5 mm) were prepared from Inconel 718 feedstock and grit blasted to a roughness of 6-8 μm. The rare earth ceramic samarium strontium aluminate (SSA) was

Table 1 Operating parameters used for atmospheric plasma spraying

	Bond coat	Top coat
Coating Powder	NiCrAlY	Al ₂ O ₃ + SSA
Coating System	APS	APS
Spray gun	MF4	MF4
Voltage	65 V	69 V
Current	500 Amp.	575 Amp.
Primary gas flow (Argon)	40 slpm	38 slpm
Secondary gas flow (Hydrogen)	6.0 slpm	8.0 slpm
Powder feed rate	40 g/min	35 g/min
Spray distance	120 mm	75 mm

Table 2 Parameters used for air jet erosion testing

Parameters	Value
Erodent	Alumina, 50 μm
Feed rate	3 g/min
Velocity	40 m/s
Temperatures	200 and 800 °C
Impingement angles	30° and 90°
Nozzle dimension	1.5 mm ID
Stand-off distance	10 mm

synthesized via molten salt synthesis from the precursor components samarium oxide, strontium oxide, and aluminum oxide. The detailed synthesis procedure is discussed in detail elsewhere (Ref 8, 15, 19). The composite top coat powder mixture (70 wt.% Al₂O₃-30 wt.% Sm₂SrAl₂O₇) was prepared from the synthesized SSA powder and high-purity alumina powder (Make: HC Starck). Commercially available NiCrAlY powder (Amdry 962 grade with observed weight percentages of Ni-64.8 %, Cr-22.5 %, Al-10.8 %, Y-1.2 %) has been used as a bond coat. The particle sizes of SSA, Alumina, and NiCrAlY used for the coating were 40, 45, and 100 μm, respectively.

2.2 Coating Development and Surface Modification

The TBC specimens were deposited by atmospheric plasma spraying using a mass flow controlled plasma system AP-2700 attached with an MF4 spray gun using the parameters listed in Table 1. The surface modification of the developed TBC specimen was carried out by deploying an Nd: YAG fiber laser. The optimized parameters 40 W power at 0.5 m/min scan speed, with a beam diameter of 500 micrometers were used to scan the coated surface.

2.3 High-Temperature Erosion Test

The as-coated (AS) and laser-treated (LS) test coupons were subjected to erosion test according to ASTM G76-13 standard using a Ducom air jet erosion tester (TR-471-800). The samples were heated to 200 and 800 °C, followed by erodent (50 μm alumina) impact at angles 30° and 90° using the parameters listed in Table 2. The erosion weight loss of the specimens was measured every 5 minutes using a Shimadzu-AUX 220 precision weighing balance, and the average erosion values were calculated.

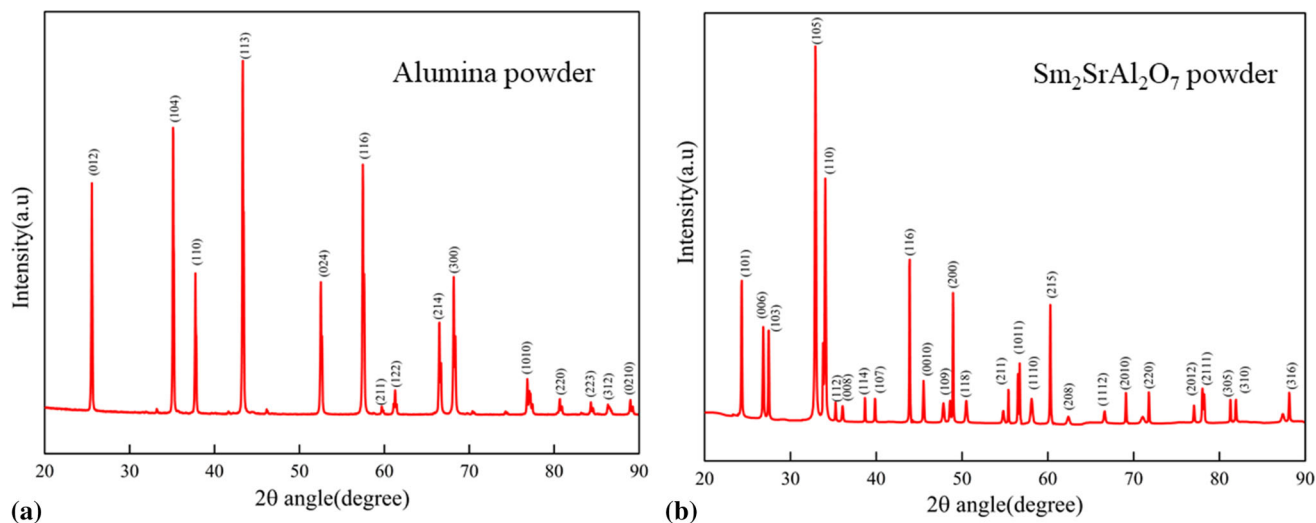


Fig. 1 XRD patterns of (a) Alumina powder (b) $\text{Sm}_2\text{SrAl}_2\text{O}_7$ powder

2.4 Characterization

The surface of the developed samples has been analyzed using an advanced x-ray diffraction (Empyrean 3rd Gen, Malvern PANalytical), and the morphology and cross-section analysis was carried out using a FESEM (7610FPLUS, Jeol). The density measurements were performed using a pycnometer of 50 mL capacity. Repeated measurements were taken and the average values are presented. The porosity of the free-standing coatings was analyzed using ImageJ software and water impregnation techniques. Only open porosities are measured and no shrinkage porosities were observed in the system. The mechanical properties such as hardness and Young's modulus of the coatings were measured through nanoindentation tests using a Berkovich diamond indenter of 20 nm tip under a maximum load of 100 mN.

3. Results and Discussion

3.1 Characterization of Coatings

The x-ray diffraction patterns (XRD) of the alumina powder showed an alpha phase with a rhombohedral structure (JCPDS No:00-042-1468) while the synthesized SSA powder showed a single-phase tetragonal structure (JCPDS No:01-074-3404), as shown in Fig. 1(a) and (b) respectively.

The free-standing coatings (without substrate) showed a pycnometer density of 4.4 g/cm^3 and an average porosity of 10 %. The Nanovea ST-400 surface profilometer measured an average surface roughness (R_a) of $6.0 \mu\text{m}$ for the as-coated samples, with $0.1 \mu\text{m}$ deviation. The nano-indentation tests showed an average hardness of 11.5 GPa and Young's modulus of 152 GPa. A standard deviation of 0.13 and 0.94 GPa was calculated for hardness and Young's modulus measurements, respectively. The cross-section of the as-coated samples showed a top coat thickness of 180-200 μm and a bond coat thickness of 75-85 μm .

As in Fig. 2(a), the morphology of the as-coated system presented a splat structure, resulting from the flattened droplets upon spraying. Upon impact on the substrate, the molten particles

flatten and solidify forming disk-shaped splats (Ref 20). The higher magnification views of the surface revealed a small fraction of microcracks on the splats, which are assumed to have originated from the thermal shock-induced stress during coating. Upon cooling after spraying, the difference in thermal expansion causes residual stress generation which may further lead to crack initiation (Ref 20). The morphology and profilometric views of the laser-treated samples showed a remelted surface, with a lower roughness of $4.0 \mu\text{m}$ as shown in Fig. 2(b) and (d). In laser-treated samples, a major portion of the surface protrusions and unmolten particles have been remelted forming a smooth surface with an improved hardness of 12.6 GPa. The presented value of hardness is the average of multiple measurements made at different locations of the sample

The as-coated top coat consisted of three phases, 29.5 % of $\text{Sm}_2\text{SrAl}_2\text{O}_7$, 53.8 % of $\text{Y-Al}_2\text{O}_3$, and 16.7 % of $\alpha\text{-Al}_2\text{O}_3$, as shown in Fig. 3(a). The SSA retained the exact phases after coating, while a major fraction of α -alumina transformed to Y -alumina upon spraying. The presence of similar dual-phase alumina was reported where the thermal spraying converted alumina from α to Y alumina (Ref 21, 22). The fraction of the phases present remained the same even after laser modification showing that the glazing did not influence the phase formation in the considered system. The glazing has caused intensity variations of individual XRD peaks, which is due to the variation in microstructure (Ref 18, 23). The SSA peak at 32.9° showed a lower intensity after the laser treatment, while the α -alumina peaks at 57.3° , 43.2° , and Y -alumina peak at 45.8° showed a higher intensity after the laser treatment. The laser-treated samples did not show SSA peaks at 50.0° and α -alumina peaks at 52.4° and 68.1° . Minor changes in the FWHM values were observed in peaks after laser remelting, as shown in Table 3. In the case of Y - alumina, the FWHM values of peaks at 31.8° and 66.8° remained the same while the peak at 45.8° showed a decrease (0.307° to 0.256°). The α -alumina peaks retained the FWHM values while the SSA peaks at 27.3° showed a decrease (0.819° to 0.614°). Only the SSA peak at 48.5° showed an increase in FWHM after laser treatment (0.409° to 0.716°). Researchers suggest that laser treatment can make significant changes in the preferred orientation of planes within the system, as observed (Ref 23).

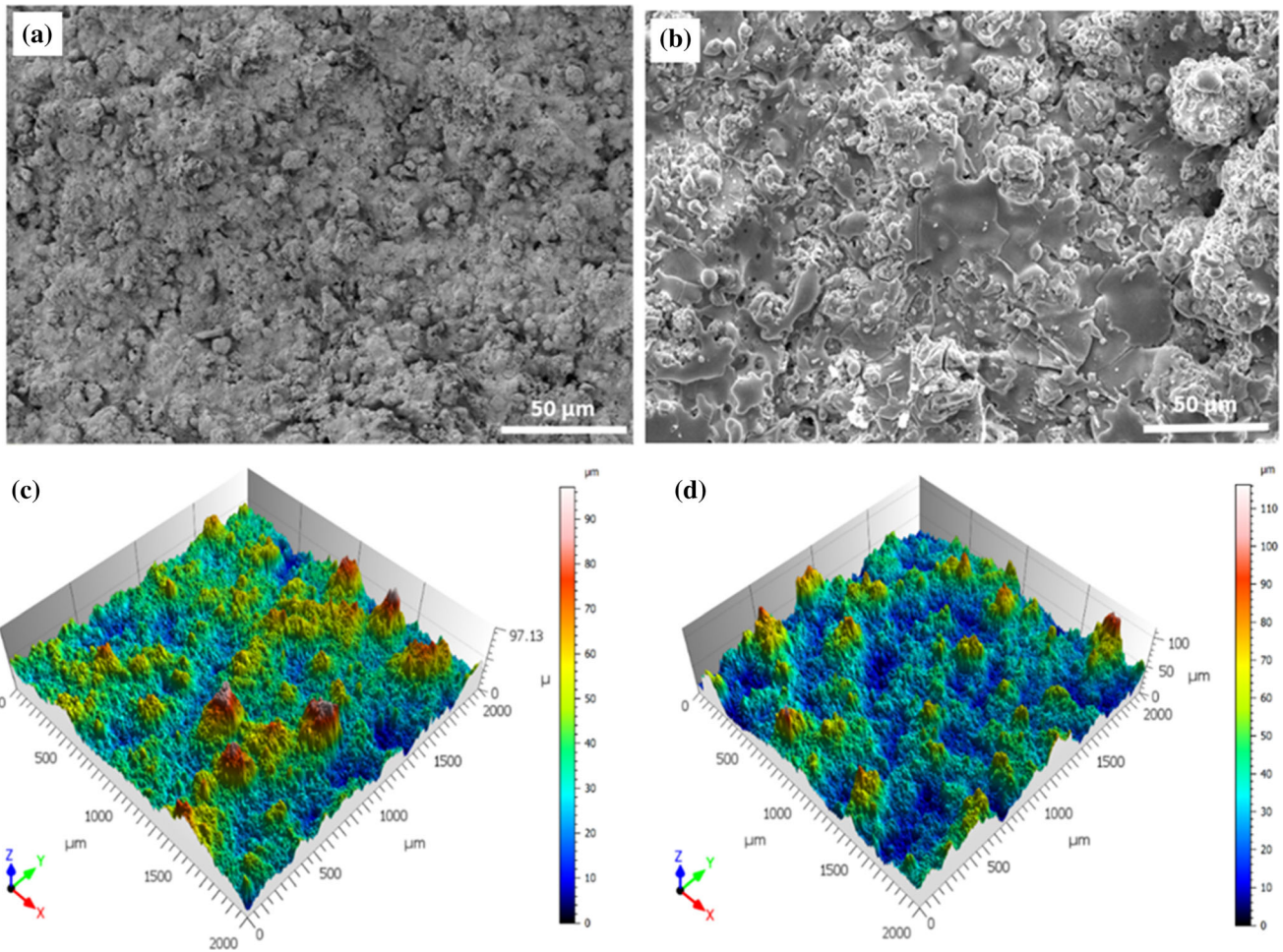


Fig. 2 Morphology and profilometric images of as-coated (a, c) and laser-treated (b, d) samples

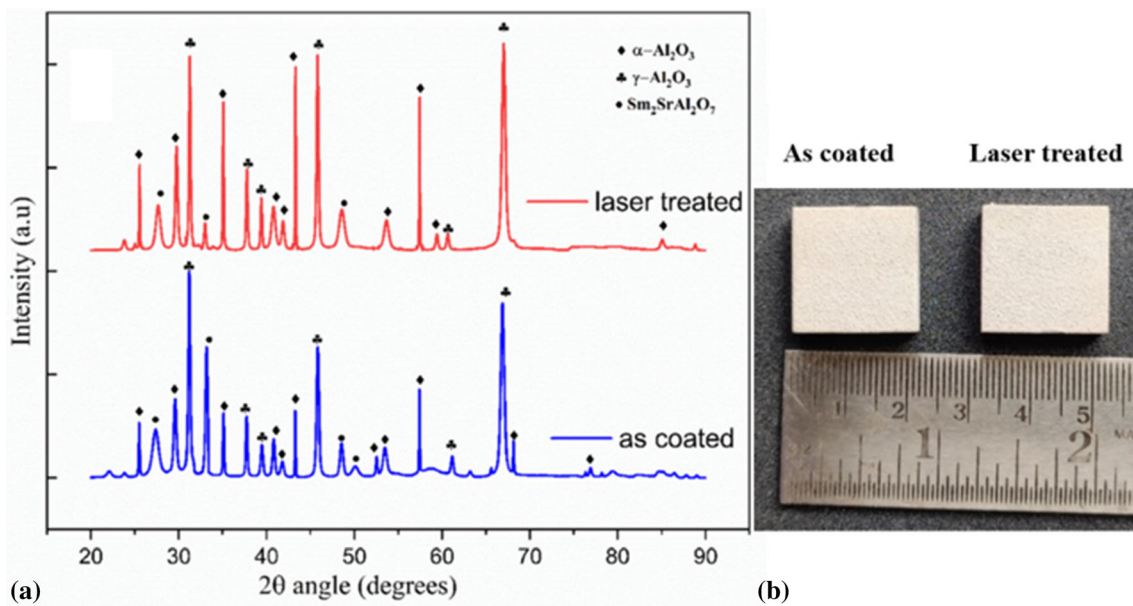


Fig. 3 (a) XRD patterns of as-coated and laser-treated sample surface (b) Photographic image of as-coated and laser-treated surfaces

3.2 Post-erosion Analysis

After 25 minutes of erosion at 200 and 800 °C, a major part of the composite coating has been chipped off. The samples underwent a localized coating removal, which appears as erosion scars, as in Fig. 4, with the dimensions shown in Table 4. At 90°, the scars presented a nearly circular area; while at 30°, the scar was nearly elliptical.

The plot of cumulative mass loss against the total mass of the erodent (Fig. 5a and b) shows that the highest mass loss was observed for as-coated samples exposed at 800 °C at a 90° impact angle. The lowest mass loss was for laser-treated samples at 200 °C at a 30° impact angle. The cumulative mass loss was comparatively lower for laser-treated samples in all conditions tested.

A higher weight loss is observed at the beginning of erodent impact due to the faster removal of surface roughness, such as protrusions on the surface. A similar trend with variation in mass loss is reported by other researchers (Ref 24). In a few samples, an increase in mass loss after 20 min (60 g) of erosion was observed, due to the flaking of particles upon crack propagation along splat interfaces. A similar observation was reported where a sharp rise in the material loss was observed over 40 g of erodent (Ref 25). In general, the volume of eroded material is proportional to the cumulative mass of erodents impacted on the coating surface (Ref 19).

3.2.1 Average Erosion Values. The average erosion values under various erosion conditions are calculated according to the ASTM standard; by dividing the erosion rate by the erodent feed rate and by the coating density. The average erosion value

was the highest for as-coated samples at 800 °C at a 90° impact angle (Fig. 5c). A minimal standard deviation of 0.00007 mm³ g⁻¹ is observed in average erosion determinations. Also, the laser-treated samples showed a comparatively lower value than the as-coated samples under all tested conditions. On average, a 7 % lower erosion loss was observed in laser-treated samples than in the as-coated samples. It is evident that at 200 and 800 °C, the erosion was maximum at a 90° than at a 30° impact angle. Generally, the transference of kinetic energy to the target surface is maximum in a normal impact (Ref 26).

3.2.2 Influence of Microstructural and Mechanical Properties on Erosion Behavior. The as-coated samples possessed an equivalent hardness as compared to single-layer YSZ, and YSZ + Al₂O₃ composite coatings (Table 5). The hardness observed is much higher than single-layer SSA coatings in as-coated conditions, due to a microstructure with lower porosity and higher alumina content. The measured hardness value was less than that of bulk alumina, which may be due to the existing porosities in the coating and a comparatively lower hardness of γ -alumina than α -alumina (Ref 20). The laser-treated samples showed an 8.7 % better hardness of 12.6 GPa, by remelting and solidification. A higher improvement in hardness was not observed, as the alumina phase fractions remained the same after laser treatment. The cooling rate after laser treatment will be higher than the cooling rate during APS coating, as only a top layer is melted during the laser treatment. During the coating process, the plasma spraying produces a larger melt pool with a

Table 3 FWHM values of major peaks in as-coated and laser-treated samples

Phases	Position, 2 θ (degrees)	FWHM, β (degrees)	
		As-coated	Laser-treated
Sm ₂ SrAl ₂ O ₇	27.3	0.819	0.614
γ -Al ₂ O ₃	31.8	0.256	0.256
α -Al ₂ O ₃	43.2	0.077	0.077
γ -Al ₂ O ₃	45.8	0.307	0.256
Sm ₂ SrAl ₂ O ₇	48.5	0.409	0.716
α -Al ₂ O ₃	57.3	0.077	0.077
γ -Al ₂ O ₃	66.8	0.461	0.461

Table 4 Scar dimensions of samples exposed to various conditions measured in a surface profilometer

	AS-800 °C	AS-200 °C	LS-800 °C	LS-200 °C
Elliptical scar (30°)				
Major diameter (mm)	5.2	2.8	3.1	2.5
Minor diameter (mm)	2.2	1.5	2.1	1.5
Circular scar (90°)				
Scar diameter (mm)	4.6	2.8	3.4	1.8

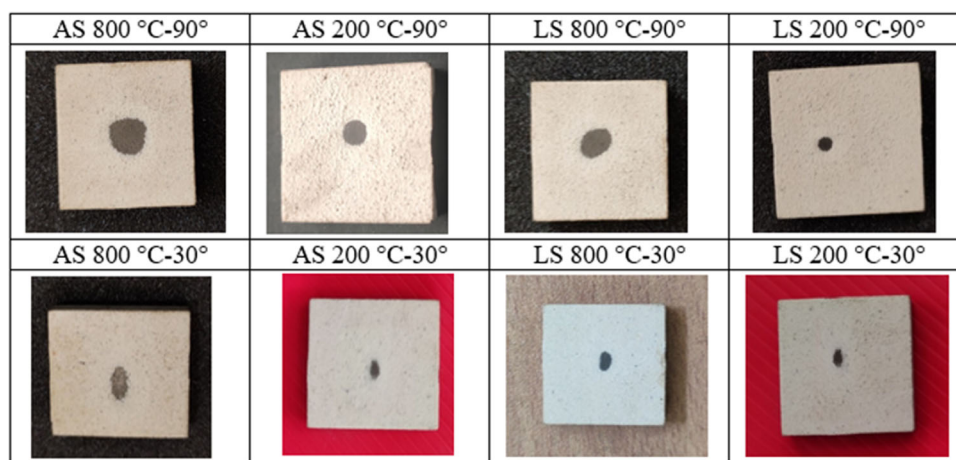


Fig. 4 Photographic images of samples exposed to erosion under various conditions

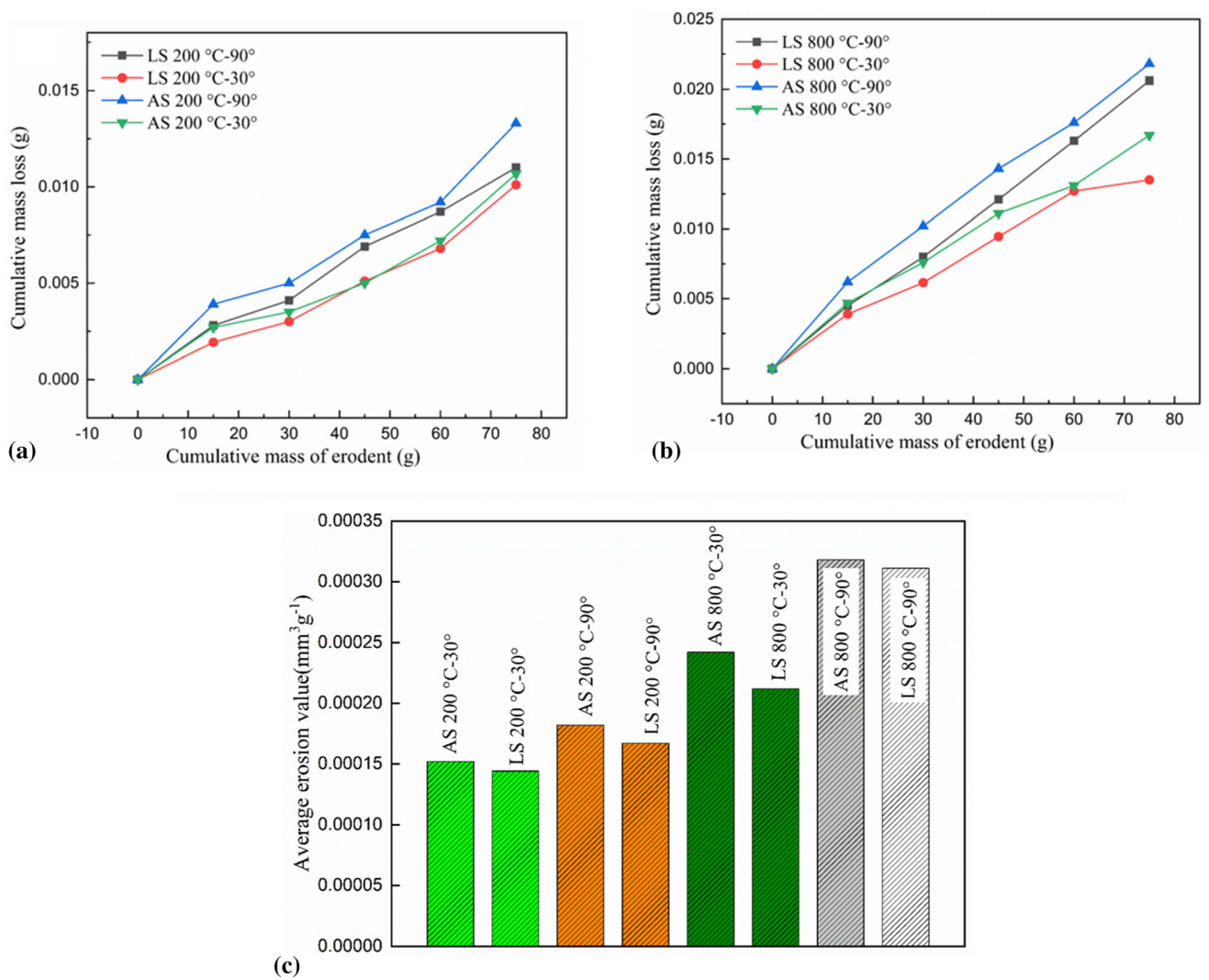


Fig. 5 (a) Graph showing cumulative mass loss of coating vs. cumulative mass of erodents for samples exposed at 200 °C and (b) 800 °C (c) Average erosion values of samples exposed to various erosive conditions

Table 5 Mechanical properties of the as-coated samples and similar systems

	Hardness	Young's modulus	References
Al ₂ O ₃ + Sm ₂ SrAl ₂ O ₇	11.5 GPa	152 GPa	Experimental
Sm ₂ SrAl ₂ O ₇	5 GPa	73 GPa	(Ref 27)
YSZ	12.26 GPa	...	(Ref 28)
50% Al ₂ O ₃ + 50% YSZ	12.7 GPa	...	(Ref 29)
Al ₂ O ₃	16 GPa	...	(Ref 30)

comparatively lower cooling rate. As there are no major changes in the phase fractions after the laser treatment, the effect of the cooling rate on the properties of the considered coatings is unrevealed.

From the EBSD analysis of the sample surfaces as shown in Fig. 6, the average grain size of laser-treated samples was about 0.0401 μm, while the as-coated samples showed an average grain size of 0.0406 μm. The difference in grain size after laser treatment is very much marginal to produce any effect on the

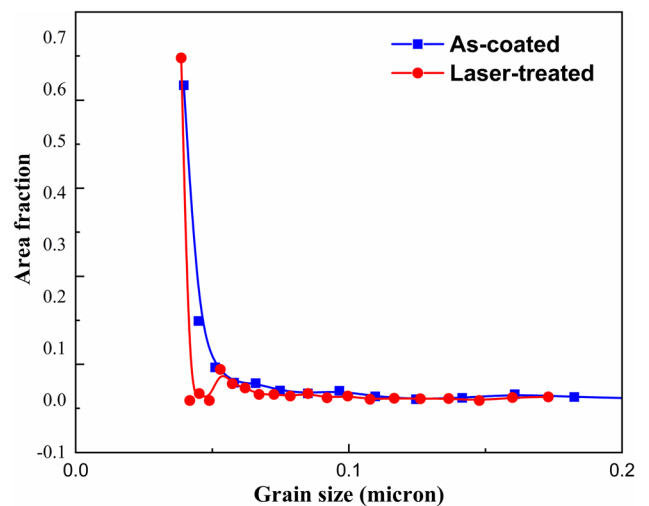


Fig. 6 Grain size distribution observed through EBSD analysis on the surface of as-coated and laser-treated sample surfaces

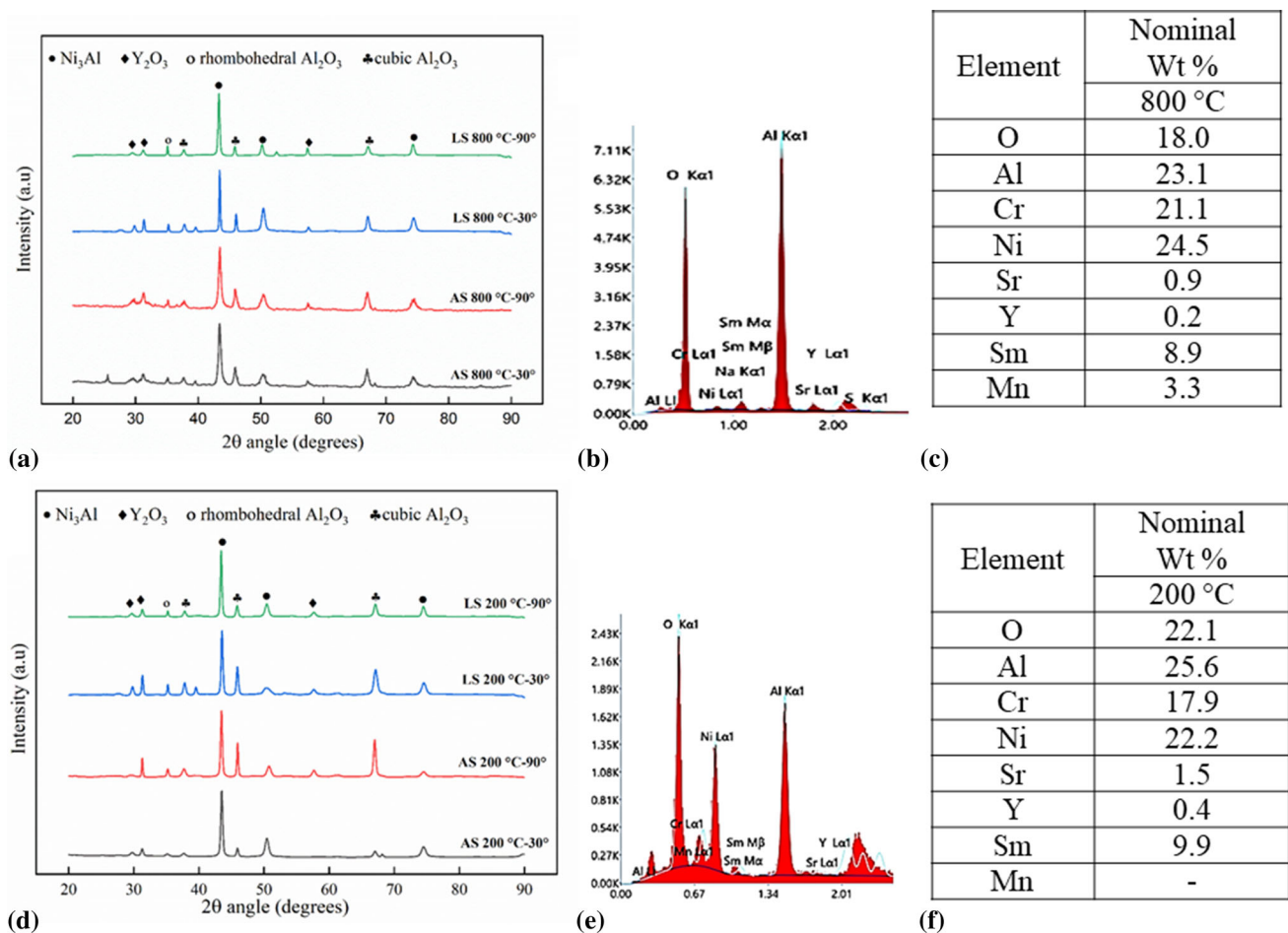


Fig. 7 (a) XRD patterns of scars in samples exposed to erosion at 800 °C (b) Nominal EDS composition of scar of as-coated samples at 800 °C and 90° impact angle and (c) EDS spectra observed on erosion scars in samples exposed to erosion at 800 °C and 90° impact angle, (d) XRD patterns of scars in samples exposed to erosion at 200 °C (e) Nominal EDS composition of scar of as-coated samples at 200 °C and 90° impact angle and (f) EDS spectra observed on erosion scars in samples exposed to erosion at 200 °C and 90° impact angle

mechanical properties of the coatings. So, the melting of protrusions and closure of surface pores played a major role in the observed improvement in hardness. It is to be noted that besides the material hardness, the indentation on plasma-sprayed coating depends on the lamellar microstructure, splats, and porosities (Ref 31, 32). In general, researchers report that TBCs with low hardness and high porosity showed a lower erosion resistance.

The erosion resistance declines with an increasing porosity level. The laser-treated samples showed a better erosion resistance than the as-coated system due to the sealing of existing open porosities. The pores existing within the microstructure reduce the thermal conductivity, while it trades off the erosion performance. The defects such as porosities and voids could bring down the effective load-bearing area upon erodent impact, and act as multiaxial stress concentrators leading to crack propagation (Ref 20). The primary erosion response of the coating system is highly dependent on the initial surface roughness of the coating, which is due to semi-molten or unmolten particles. The more completely molten particles enhance the intersplat bonding, reduce porosity, and improve the surface roughness. A reduced surface roughness controls the effective area of contact with the abrasive particle jet (Ref 21). With the onset of erodent impact, the surface protuberances and asperities are fractured and removed, reflecting a rapid weight loss (Ref 24). The laser glazing reduces surface

roughness by re-engineering the top surface via remelting and enhances the component life.

In ceramic coatings, the quenching stress is often relieved by splat microcracking, which degrades the erosion resistance, paving the way for the chipping of the coating upon erodent impact (Ref 26). The laser remelting may contribute to the closing of the existing micro-cracks on the surface.

3.2.3 Characterization of Erosion Scars. The XRD patterns of the erosion scars observed in as-coated and laser-treated samples at 800 and 200 °C are shown in Fig. 7(a) and (d). The patterns showed both the top coat and bond coat elements, proving that a major fraction of the top coat is removed, exposing areas of the bond coat. The patterns presented intensity variations due to the microstructural non-uniformity of the eroded areas.

In the case of erosion at 800 °C and 90° impact angle, the major peak at 43.4° showed a higher FWHM value in as-coated samples (0.307°) than laser-treated samples (0.281°). A similar decrease in FWHM value was observed in laser-treated samples (0.154°) than in as-coated samples (0.256°) after erosion at 800 °C at a 30° impact angle.

A comparable trend with reduced FWHM values in laser-treated samples than as-coated samples was observed in scars of samples exposed to erosion at 200 °C, at both 30° and 90° impact angles. Overall, at every condition tested, a higher

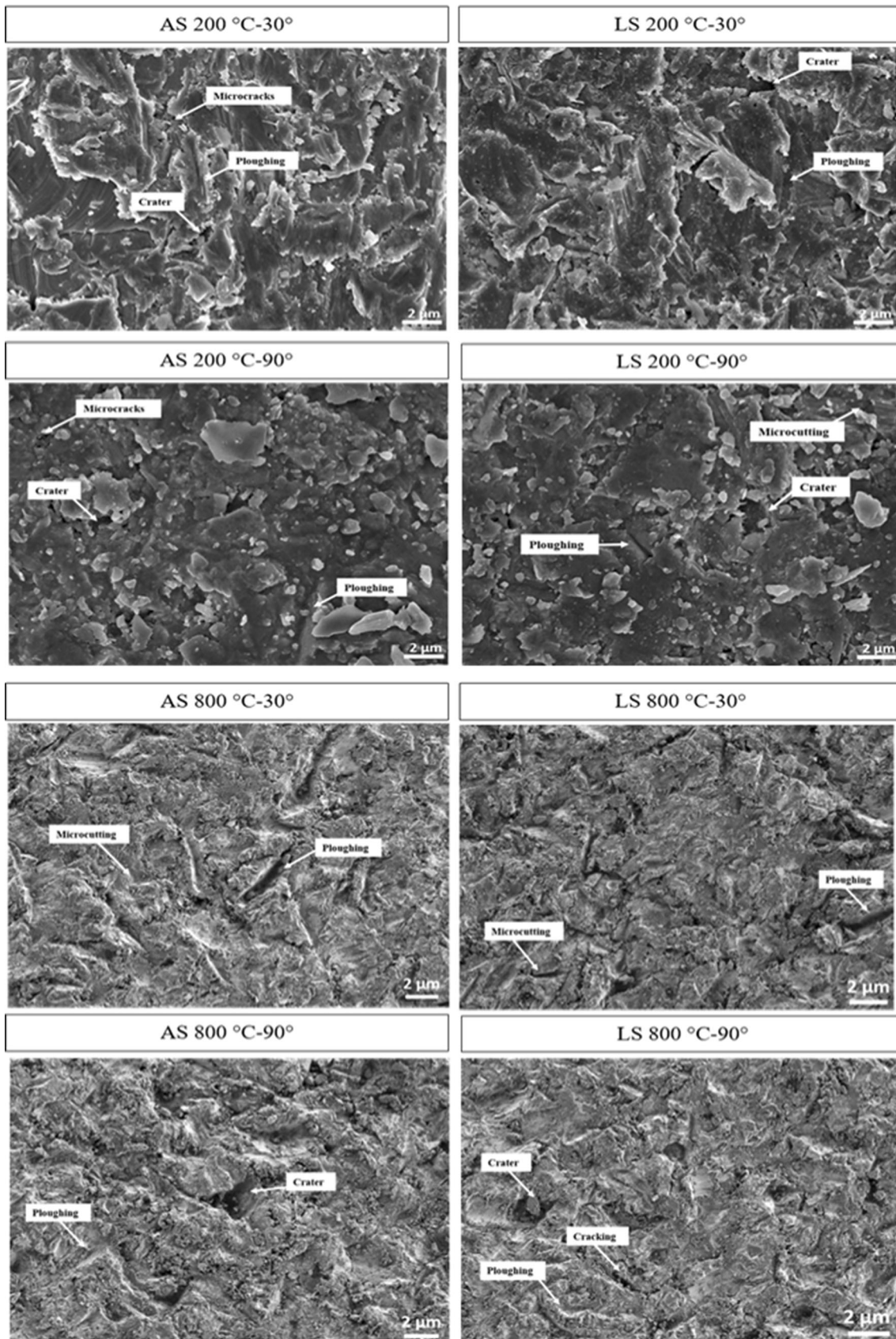


Fig. 8 High magnification SEM images of erosion scars in samples exposed to various erosive conditions

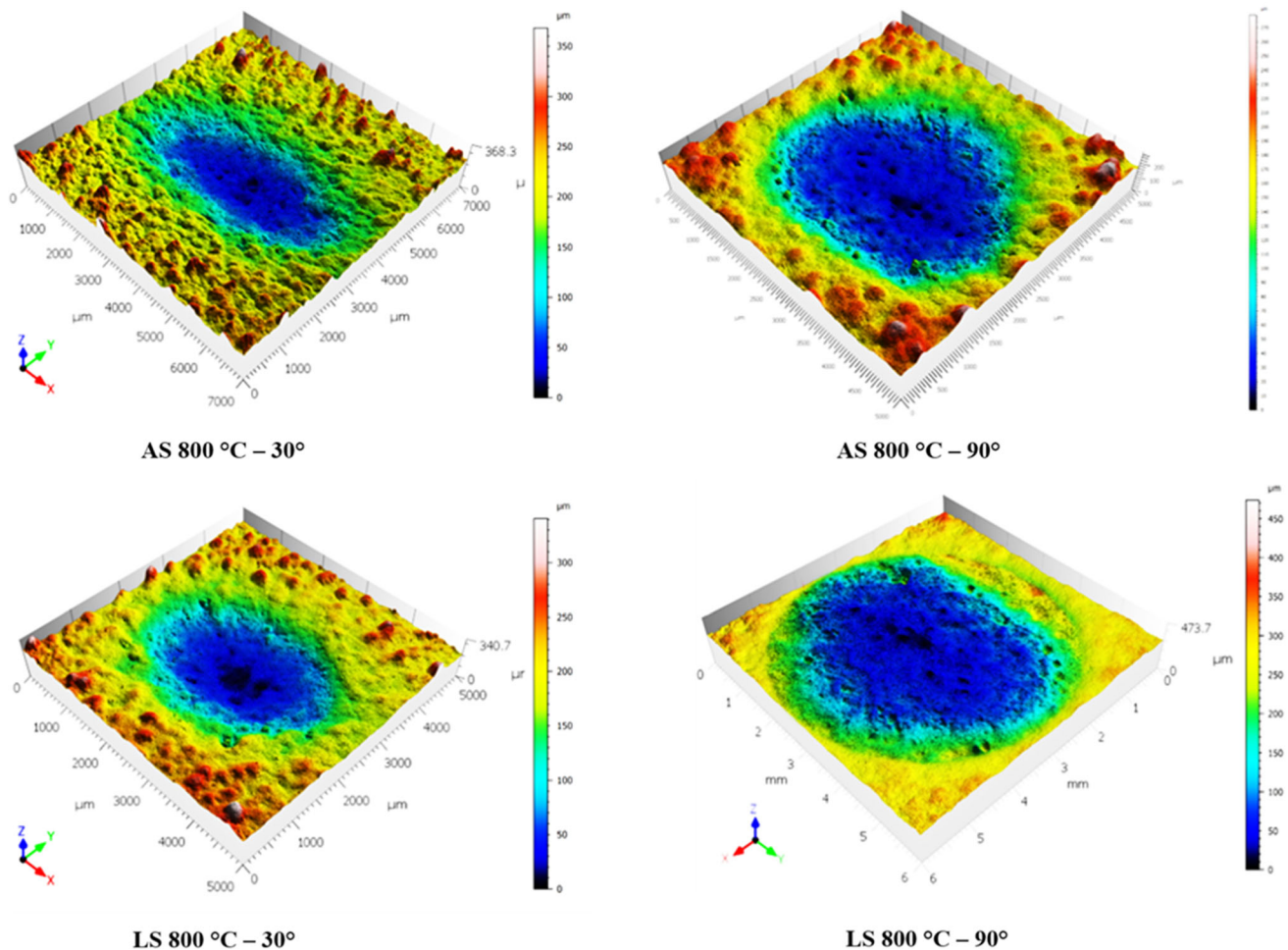


Fig. 9 Profilometric views of erosion scars in as-coated and laser-treated samples exposed to erosion at 800 °C

FWHM shows a higher stress induced in as-coated samples than the laser-treated samples.

The EDS analysis of erosion scars in as-coated and laser-treated samples also showed the presence of both the top coat and bond coat elements (Fig. 7b and e). The microstructure of erosion scars in the eroded samples is shown in Fig. 8. The scars in as-coated samples at 800 °C showed deeper and longer plowing marks, revealing a ductile mechanism involved. From the worn surfaces, it can be assumed that more material is removed by plowing at 800 °C. The mechanism observed can be defined as microplowing, which can cause material removal in coatings. Various research reports deformation and coating removal by plowing. Micro-cutting, micro-cracks, and grooves are also observed in the scar, pointing to the brittle mechanisms. At 800 °C deeper craters are observed at 90° than 30° impact angle, due to the higher kinetic energy imparted into the heated-up coating, allowing deeper penetration. The laser-treated samples also showed similar features of microcracks, micro-cutting, and craters, pointing an identical material removal, at a lower magnitude. Earlier reports suggest that laser-treated surfaces possess a better damage tolerance than as-coated surfaces (Ref 33).

For as-coated samples at 200 °C, the degree of plowing and material removal is lesser with shallow plowing channels as compared to 800 °C. Microcracks and smaller craters are visible in the eroded area. The brittle mechanisms are observed

to be more dominant at 200 °C than 800 °C, with comparatively higher magnitude at 90° than at 30°.

From the profilometric analysis as shown in Fig. 9, a larger and deeper erosion scar profile is observed in as-coated samples exposed to 800 °C at 90°, while the laser-treated samples showed slightly smaller erosion scars under the same conditions.

3.3 Comprehensive Erosion Behavior

In both the as-coated and laser-treated samples, though there are mechanisms suggesting ductility, the mass monitoring did not show any negative erosion and subsequent mass gain, eradicating the possibility of any clinging mechanisms involved. A higher erosion at a 30° impact angle than 90° is generally a behavior of ductile materials, while brittle coatings erode more at 90°. The single-layer $\text{Sm}_2\text{SrAl}_2\text{O}_7$ ceramic TBC reports a ductile behavior with maximum erosion at a 30° impact angle, which is contrary to the considered composite coatings. On the other hand, single-layer alumina coatings exhibit a brittle behavior with higher erosion damage at 90° (Ref 26). It can be assumed that the introduction of ductile $\text{Sm}_2\text{SrAl}_2\text{O}_7$ phase to the brittle alumina altered the overall failure mechanism to a mixed mode of material removal. Introducing a ductile phase into the alumina matrix could relax

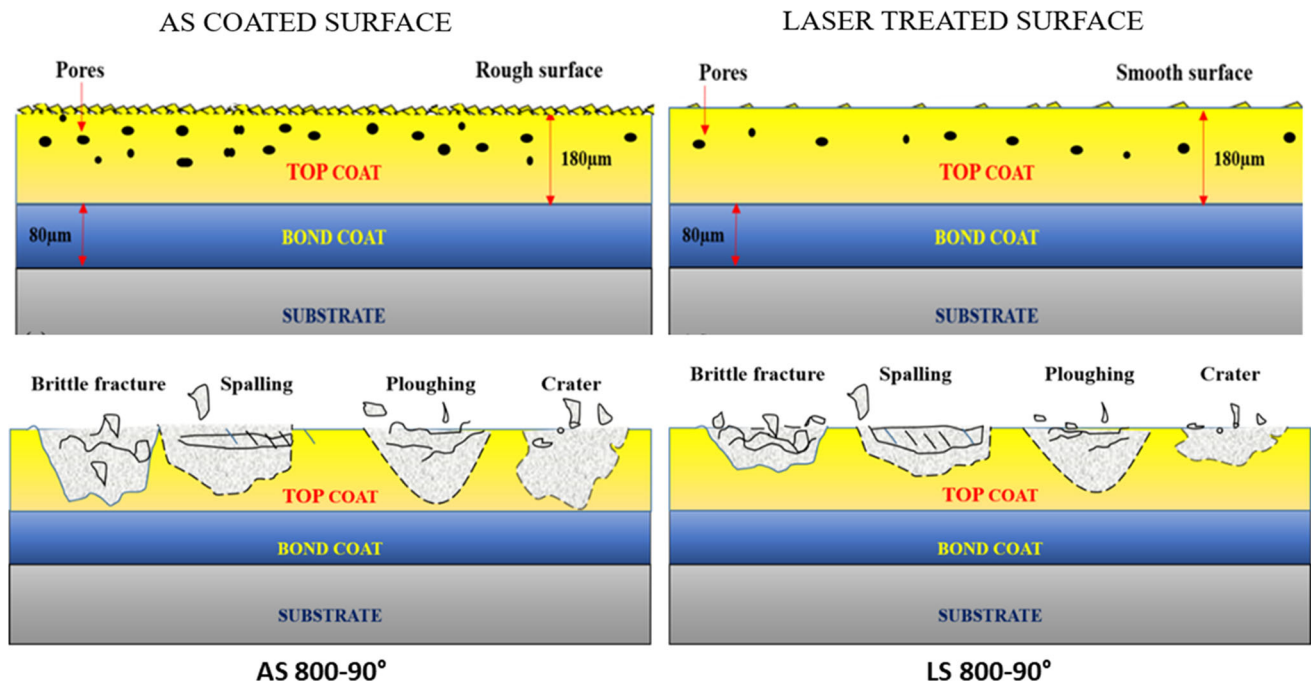


Fig. 10 Schematic diagram of erosion mechanisms observed in as-coated and laser-treated samples at 800 °C (not in scale)

the stresses by yielding and delaying cracking failure (Ref 26). Figure 10 illustrates the erosion mechanism presented by as-coated and laser-treated samples at 800 °C. At 800 °C at 90°, deeper craters were observed for as-coated samples while the laser-treated samples showed slightly lower craters. All the samples showed spallation of lamellas upon erosion.

A comparison of the as-coated and laser-treated samples shows that there are no remarkable differences in the failure mechanisms involved. Considering the average erosion values of all the samples, the laser-treated samples showed 7% lower erosion than the as-coated samples. The laser-treated coating, with better surface roughness and lesser porosities, resists erosion slightly better than the as-coated samples. The comparatively dense layer after re-solidification offers increased resistance to impact. Thus, optimizing the laser treatment on the composite samples, considering multiple factors such as reduction in porosity, surface roughness, and cracking tendencies, can offer a higher degree of resistance to the system.

4. Conclusion

- In the developed 70 wt.% alumina-30 wt.% samarium strontium aluminate composite coatings, a mixed mode of erosion is observed under the tested conditions.
- The introduction of rare earth ceramic $\text{Sm}_2\text{SrAl}_2\text{O}_7$ into the brittle alumina matrix reduced the brittle fracture mechanisms.
- At 200 and 800 °C, maximum erosion was observed at a 90° impact angle, which states that the brittle behavior dominates in the erosion failure.
- The laser treatment provides better erosion resistance to the coatings at both low and high temperatures.

- The laser-treated samples showed 7% lower erosion than the as-coated samples due to a decrease in surface roughness and an increase in hardness.

Acknowledgments

The authors would like to thank the Central Research Facility (CRF), NITK for providing the characterization facilities. The authors would like to thank the Mechanical Engineering Department, Ramaiah Institute of Technology, Bangalore for availing of the air jet erosion test facility.

References

1. A.G. Davis, D.H. Boone, and A.V. Levy, Erosion of Ceramic Thermal Barrier Coatings, *Wear*, 1986, **110**, p 101–116.
2. F. Cernuschi, L. Lorenzoni, S. Capelli, C. Guardamagna, M. Karger, R. Vaßen, K. von Niessen, N. Markocsan, J. Menuey, and C. Giolli, Solid Particle Erosion of Thermal Spray and Physical Vapour Deposition Thermal Barrier Coatings, *Wear*, 2011, **271**(11–12), p 2909–2918. <https://doi.org/10.1016/j.wear.2011.06.013>
3. J.H. Ouyang and S. Sasaki, Microstructure and Tribological Characteristics of $\text{ZrO}_2\text{-Y}_2\text{O}_3$ Ceramic Coatings Deposited by Laser-Assisted Plasma Hybrid Spraying, *Tribol. Int.*, 2002, **35**(4), p 255–264.
4. L. Luo, Y. Chen, M. Zhou, X. Shan, J. Lu, and X. Zhao, Progress Update on Extending the Durability of Air Plasma Sprayed Thermal Barrier Coatings, *Ceram. Int.*, 2022, **48**(13), p 18021–18034. <https://doi.org/10.1016/j.ceramint.2022.04.044>
5. X. Song, Z. Liu, M. Kong, C. Lin, L. Huang, X. Zheng, and Y. Zeng, Thermal Stability of Yttria-Stabilized Zirconia (YSZ) and YSZ- Al_2O_3 coatings, *Ceram. Int.*, 2017, **43**(16), p 14321–14325. <https://doi.org/10.1016/j.ceramint.2017.07.186>
6. C.S. Ramachandran, V. Balasubramanian, and P.V. Ananthapadmanabhan, Erosion of Atmospheric Plasma Sprayed Rare Earth Oxide

- Coatings under Air Suspended Corundum Particles, *Ceram. Int.*, 2013, **39**(1), p 649–672. <https://doi.org/10.1016/j.ceramint.2012.06.077>
7. L. Jia, T. Wen, C. Tian, Z. Liu, J. Yu, and L. Yuan, Preparation and Thermophysical Properties of RE₂CrTaO₇ (Y, Sm, Dy, Yb) Ceramics for Thermal Barrier Coating Applications, *Ceram. Int.*, 2022, **48**(16), p 23814–23820. <https://doi.org/10.1016/j.ceramint.2022.05.036>
 8. T. Baskaran and S.B. Arya, Role of Thermally Grown Oxide and Oxidation Resistance of Samarium Strontium Aluminate Based Air Plasma Sprayed Ceramic Thermal Barrier Coatings, *Surf. Coat. Technol.*, 2017, **326**, p 299–309. <https://doi.org/10.1016/j.surfcoat.2017.07.049>
 9. T. Baskaran and S.B. Arya, Hot Corrosion Resistance of Air Plasma Sprayed Ceramic Sm₂SrAl₂O₇ (SSA) Thermal Barrier Coatings in Simulated Gas Turbine Environments, *Ceram. Int.*, 2018, **7**(15), p 17695–17708. <https://doi.org/10.1016/j.ceramint.2018.06.234>
 10. T. Baskaran and S.B. Arya, Fabrication of Samarium Strontium Aluminate Ceramic and Deposition of Thermal Barrier Coatings by Air Plasma Spray Process, *MATEC Web Conf.*, 2018, **144**, p 1–8.
 11. S. Mahade, N. Curry, S. Björklund, N. Markocsan, P. Nylén, and R. Vaßen, Erosion Performance of Gadolinium Zirconate-Based Thermal Barrier Coatings Processed by Suspension Plasma Spray, *J. Therm. Spray Technol.*, 2017, **26**(1–2), p 108–115.
 12. R. Westergård, L.C. Erickson, N. Axén, H.M. Hawthorne, and S. Hogmark, The Erosion and Abrasion Characteristics of Alumina Coatings Plasma Sprayed under Different Spraying Conditions, *Tribol. Int.*, 1998, **31**(5), p 271–279.
 13. A. Avci, A. Akdogan Eker, and M. Karabas, An Investigation of Oxidation, Hot Corrosion, and Thermal Shock Behavior of Atmospheric Plasma Sprayed YSZ-Al₂O₃ Composite Thermal Barrier Coatings, *Int. J. Mater. Res.*, 2020, **111**, p 1–14.
 14. H. Xu and H. Guo, *Thermal Barrier Coatings*, Woodhead Publishing in Materials, Cambridge, 2011
 15. F.J. Joseph, S.B. Arya, and S. Tailor, Hot Corrosion Behavior Of Al₂O₃ + Sm₂SrAl₂O₇ Composite Thermal Barrier Coatings, *Mater. Corros.*, 2022, **73**(12), p 2004–2008.
 16. M.S. Reza, S.N. Aqida, and I. Ismail, Laser Surface Modification of Yttria Stabilized Zirconia (YSZ) Thermal Barrier Coating on AISI H13 Tool Steel Substrate, *IOP Conf. Ser. Mater. Sci. Eng.*, 2018, **319**(1), p 012067.
 17. Y. Feng, T.S. Dong, G.L. Li, R. Wang, G.Z. Ma, X.W. Zhao, and Q. Liu, The Roles of Stress in the Thermal Shock Failure of YSZ TBCs Before and After Laser Remelting, *J. Alloys Compd.*, 2020, **828**, p 154417. <https://doi.org/10.1016/j.jallcom.2020.154417>
 18. R. Ghasemi, R. Shoja-Razavi, R. Mozafarinia, and H. Jamali, The Influence of Laser Treatment on Thermal Shock Resistance of Plasma-Sprayed Nanostructured Yttria Stabilized Zirconia Thermal Barrier Coatings, *Ceram. Int.*, 2014, **40**(1), p 347–355. <https://doi.org/10.1016/j.ceramint.2013.06.008>
 19. J. Fredy James, S.B. Arya, and S. Tailor, Erosion Behavior of Al₂O₃ + Sm₂SrAl₂O₇ Composite Thermal Barrier Coatings, *Mater. Today Proc.*, 2022, **66**, p 3853–3858. <https://doi.org/10.1016/j.matpr.2022.06.294>
 20. N. Krishnamurthy, M.S. Murali, B. Venkataraman, and P.G. Mukunda, Characterization and Solid Particle Erosion Behavior of Plasma Sprayed Alumina and Calcia-Stabilized Zirconia Coatings on Al-6061 Substrate, *Wear*, 2012, **274–275**, p 15–27. <https://doi.org/10.1016/j.wear.2011.08.003>
 21. D. Wang, Z. Tian, L. Shen, Z. Liu, and Y. Huang, Effects of Laser Remelting on Microstructure and Solid Particle Erosion Characteristics of ZrO₂-7wt%Y₂O₃ Thermal Barrier Coating Prepared by Plasma Spraying, *Ceram. Int.*, 2014, **40**(6), p 8791–8799. <https://doi.org/10.1016/j.ceramint.2014.01.101>
 22. P.P. Psyllaki, M. Jeandin, and D.I. Pantelis, Microstructure and Wear Mechanisms of Thermal-Sprayed Alumina Coatings, *Mater. Lett.*, 2001, **47**(January), p 77–82.
 23. P.C. Tsai, J.H. Lee, and C.L. Chang, Improving the Erosion Resistance of Plasma-Sprayed Zirconia Thermal Barrier Coatings by Laser Glazing, *Surf. Coatings Technol.*, 2007, **202**(4–7), p 719–724.
 24. M.J. Presby and B.J. Harder, Solid Particle Erosion of a Plasma Spray—Physical Vapor Deposition Environmental Barrier Coating in a Combustion Environment, *Ceram. Int.*, 2021, **47**(17), p 24403–24411. <https://doi.org/10.1016/j.ceramint.2021.05.154>
 25. C. Li, G. Yang, and A. Ohmori, Relationship Between Particle Erosion and Lamellar Microstructure for Plasma-Sprayed Alumina Coatings, *Wear*, 2006, **260**, p 1166–1172.
 26. D.A.J. Ramm, M. Hutchings, and T.W. Clyne, Erosion Resistance and Adhesion of Composite Metal/Ceramic Coatings Produced by Plasma Spraying, *J. Phys.*, 1993, **3**(7), p 913–919.
 27. T. Baskaran, *Synthesis and Development of Sm₂SrAl₂O₇ Based Air Plasma Sprayed Ceramic Thermal Barrier Coatings: Oxidation, Hot Corrosion and High Temperature Erosion Study*, 2018
 28. M. Ramesh and K. Marimuthu, Microstructural, Thermal and Wear Behavior of YSZ/Al₂O₃ Thermal Barrier Coatings for Gun Barrel Applications, *Dig. J. Nanomater. Biostruct.*, 2020, **15**(2), p 527–536.
 29. U. Saral and N. Toplan, Thermal Cycle Properties of Plasma Sprayed YSZ/Al₂O₃ Thermal Barrier Coatings, *Surf. Eng.*, 2009, **25**(7), p 541–547.
 30. T. Lampke, D. Meyer, G. Alisch, B. Wielage, H. Pokhmurska, M. Klappkiv, and M. Student, Corrosion and Wear Behavior of Alumina Coatings Obtained by Various Methods, *Mater. Sci.*, 2011, **46**(5), p 591–598.
 31. W. Caroline, *Erosion Behaviour of Thermal Barrier Coatings*, Linköping University, 2021
 32. V. Matikainen, K. Niemi, H. Koivuluoto, and P. Vuoristo, Abrasion, Erosion and Cavitation Erosion Wear Properties of Thermally Sprayed Alumina Based Coatings, *Coatings*, 2014, **4**(1), p 18–36.
 33. S. Ahmaniemi, P. Vuoristo, and T. Mäntylä, Mechanical and Elastic Properties of Modified Thick Thermal Barrier Coatings, *Mater. Sci. Eng. A*, 2004, **366**(1), p 175–182.

Publisher's Note Springer Nature remains neutral with regard to jurisdictional claims in published maps and institutional affiliations.

Springer Nature or its licensor (e.g. a society or other partner) holds exclusive rights to this article under a publishing agreement with the author(s) or other rightsholder(s); author self-archiving of the accepted manuscript version of this article is solely governed by the terms of such publishing agreement and applicable law.